Translational Oncology 64 (2026) 102663

Contents lists available at ScienceDirect

Translational Oncology

journal homepage: www.elsevier.com/locate/tranon

Integrated spatial and single-cell transcriptomics reveals RPL8 as a prognostic biomarker and therapeutic target in hepatocellular carcinoma

Jinna Tan [a,c,†], Junzhu Liang [a,†], Yaoyang Li [a], Jiaqian He [a,c], Hui Yin [a,c], Hemeng Wu [b], Yuzhen Luo [b], Mingfen Li [b,‡], Fuli Long [d,‡], Hongsheng Lin [b,‡,*]

[a] Guangxi University of Chinese Medicine, Nanning 530200, China
[b] Clinical Laboratory Department, The First Affiliated Hospital, Guangxi University of Chinese Medicine, Nanning, 530023, China
[c] First Clinical Medical College, Guangxi University of Chinese Medicine, Nanning, 530022, China
[d] Department of Hepatology, The First Affiliated Hospital of Guangxi University of Chinese Medicine, Nanning, 530023, China

ARTICLE INFO

Keywords:
Hepatocellular carcinoma
RPL8
Single cell sequencing
Spatial transcriptomics
Biomarker
Integrated multi-omics analysis

ABSTRACT

Background & aims: Ribosomal protein L8 (RPL8) is up-regulated in hepatocellular carcinoma (HCC), yet its clinical value and microenvironment role remain unclear.
Methods: Multi-omics (TCGA, CPTAC), scRNA-seq (GSE146115) and spatial transcriptomics were integrated; function was tested by RPL8 knockdown, proliferation/migration assays and drug-sensitivity screens.
Results: RPL8 mRNA/protein were markedly elevated ($p < 0.001$) with AUC 0.95 for diagnosis. High RPL8 independently predicted shorter overall (HR 1.42) and disease-specific survival (HR 1.35). Mechanistically, RPL8 co-activated MYC/G2M signaling, rewired glutathione metabolism and correlated with cell-cycle/DNA-repair scores ($p < 0.001$). scRNA-seq showed selective RPL8 enrichment in malignant hepatocytes and exhausted $CD8^+$ *T* cells; spatial maps revealed tumor-confined expression inversely linked to immune infiltration ($p < 0.01$). Silencing RPL8 suppressed proliferation, migration and glutathione synthesis ($p < 0.001$), while sensitizing cells to sirolimus and sclareol ($p < 0.05$).
Conclusions: RPL8 drives HCC progression and immune evasion, qualifying it as a diagnostic biomarker and therapeutic target.

Introduction

HCC represents a significant global health burden, comprising 80–90 % of primary liver cancers and ranking as the fourth leading cause of cancer-related mortality worldwide [1]. The disease's high morbidity and mortality rates stem from its complex multifactorial etiology, which includes chronic hepatitis B (HBV) and C (HCV) infections, aflatoxin exposure, alcohol abuse, and metabolic dysfunction-associated steatohepatitis (MASH) [2–6]. Despite improved surveillance strategies, approximately 70 % of cases are diagnosed at advanced stages when curative interventions become unavailable [7]. A persistent diagnostic dilemma remains the lack of reliable biomarkers, as current gold-standard markers such as α-fetoprotein (AFP) demonstrate suboptimal performance in clinical practice [8,9]. This critical diagnostic gap highlights the urgent need for novel molecular markers with improved accuracy for early detection and prognostic evaluation in HCC management.

Ribosomal proteins (RPs) are essential not only for protein synthesis but also for regulating diverse cellular processes, including transcription, apoptosis, and DNA repair [10]. Among them, ribosomal protein L8 (RPL8), a core component of the 60S ribosomal subunit, has emerged as a multifunctional regulator with both canonical and extraribosomal roles. Structurally, RPL8 contributes to ribosome assembly and stability [11]. Functionally, it modulates key oncogenic pathways, including mTORC1 signaling and selective mRNA translation [12,13]. Notably, RPL8 is frequently dysregulated in cancers such as osteosarcoma [14] and hepatocellular carcinoma [15], where it promotes tumor progression through enhanced protein synthesis and apoptosis evasion. These findings highlight RPL8 as a critical player in oncogenesis, bridging ribosome biology with cancer-specific regulatory mechanisms.

* Corresponding author at: The First Affiliated Hospital of Guangxi University of Chinese Medicine CHINA.
E-mail address: linhs@gxtcmu.edu.cn (H. Lin).
† These authors contributed equally to this work.
‡ Mingfen Li, Fuli Long and Hongsheng Lin contributed equally.

https://doi.org/10.1016/j.tranon.2025.102663
Received 17 October 2025; Received in revised form 9 December 2025; Accepted 22 December 2025
Available online 6 January 2026

In recent years, the therapeutic paradigm for advanced HCC has evolved from single-agent tyrosine kinase inhibitors to combination regimens incorporating immune checkpoint inhibitors, which have improved patient survival [16,17]. Nonetheless, primary and acquired resistance to these therapies remains a major clinical obstacle [18]. This persistent challenge, coupled with the diagnostic limitations of current biomarkers, underscores the urgent need to identify novel molecular targets that are not only prognostically informative but also functionally implicated in therapy response.

Despite recent advances, our understanding of the expression landscape, prognostic value, and mechanistic roles of RPL8 in HCC remains fragmentary. To fill these gaps, we leveraged single-cell and spatial transcriptomics to map RPL8 across proliferative and transcriptomic states within the HCC tumor cycle and to delineate its spatial topography. By elucidating the oncogenic circuitry governed by RPL8, this study aims to generate actionable insights for the identification of robust clinical biomarkers and the development of HCC-specific targeted therapies, as outlined in Fig. 1.

Materials and methods

Data sources and preprocessing

RNA-seq (TPM) data from the TCGA-Liver Hepatocellular Carcinoma (TCGA-LIHC) cohort were obtained from the NCI Genomic Data Commons portal (https://portal.gdc.cancer.gov). Expression microarray or RNA-seq datasets GSE146115, GSE112790, GSE10141, GSE104580, GSE109211, GSE113996, GSE116174, GSE144269, GSE14520, GSE39791, GSE54236, and GSE76427 were downloaded from the NCBI Gene Expression Omnibus (GEO, https://www.ncbi.nlm.nih.gov/geo). The E-TABM-36 series was retrieved from ArrayExpress (https://www.ebi.ac.uk/arrayexpress/experiments/E-TABM-36), and the ICGC-LIRI cohort from the International Cancer Genome Consortium (https://dcc.icgc.org/projects/LIRI-JP). All datasets are accompanied by comprehensive clinical annotations for HCC patients.

Pan-cancer expression profiling

Gene expression analysis was performed using the standardized TCGA PanCanAtlas dataset (EBPlusPlusAdjustPANCAN_IlluminaHiSeq_RNASeqV2.geneExp.tsv). Expression values underwent Z-score normalization, followed by systematic exclusion of outliers ($|Z\text{-score}| > 3$) to ensure data quality. To maintain analytical robustness, we restricted our analysis to cancer types containing at least three matched normal-tumor pairs. Differential expression between malignant and adjacent normal tissues in gastrointestinal cancers was statistically assessed using the non-parametric Wilcoxon rank-sum test.

Protein expression profiles were acquired from the Clinical Proteomic Tumor Analysis Consortium (CPTAC) database. Prior to analysis, proteins with missing values were filtered out, and samples were categorized into tumor and normal groups based on established clinical annotations. Comparative analysis between groups was conducted using Wilcoxon rank-sum tests, with results visualized through box plots depicting median values, interquartile ranges, and outlier distributions.

Furthermore, we employed the pROC package in R to conduct receiver operating characteristic (ROC) curve analysis. Diagnostic performance was quantified by calculating the area under the curve (AUC) with 95 % confidence intervals (CIs), with the following interpretive thresholds: AUC > 0.7 (moderate discriminatory power), > 0.8 (good), and > 0.9 (excellent).

Prognostic analysis of RPL8 in hepatocellular carcinoma

We employed a multistage survival analysis approach to systematically evaluate the prognostic significance of RPL8 in hepatocellular carcinoma. The analysis pipeline consisted of the following steps:

First, the optimal cutoff value for RPL8 gene expression stratification was determined using the survminer package (version 0.4.9), with the constraint that each expression group (high vs. low) contained at least 30 % of the total samples. Survival outcomes between these predefined groups were then compared using Kaplan-Meier survival analysis, with statistical significance assessed by the log-rank test (significance threshold set at $p < 0.05$).

Subsequently, we performed univariate Cox proportional hazards regression to quantify the association between RPL8 expression levels and patient prognosis. To enhance the robustness of our findings, we conducted a meta-analysis of multicenter datasets using the meta package (v5.2–0), implementing a random-effects model to calculate pooled hazard ratios (HRs) with corresponding 95 % confidence intervals (CIs). Study heterogeneity was evaluated using the I^2 statistic, with $I^2 > 50$ % considered indicative of substantial heterogeneity.

Finally, we constructed a multivariable Cox regression model to adjust for potential confounding factors, incorporating RPL8 expression levels along with key clinicopathological variables including age, gender, and TNM stage. All statistical analyses were performed using R software (version 4.2.0; R Foundation for Statistical Computing), with results visualized using the forestplotter package (version 0.2.0).

Differential expression analysis, gene set enrichment analysis, and functional state assessment

Samples were stratified into RPL8 high-expression (top 30 %) and

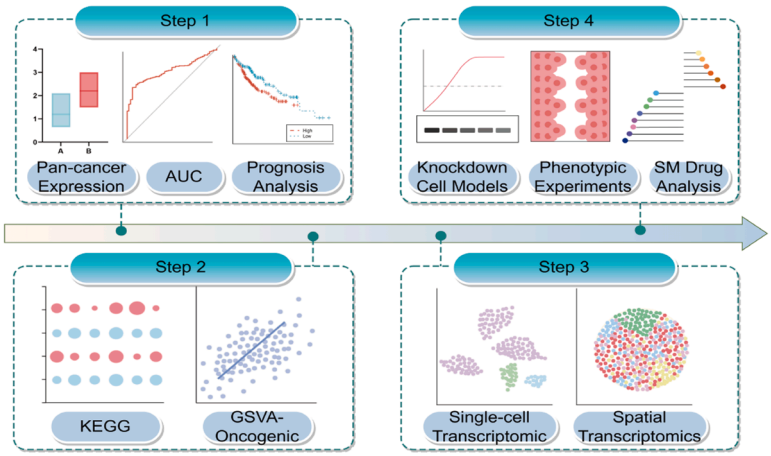

Fig. 1. Graphical abstract.

low-expression (bottom 30 %) cohorts based on mRNA expression levels. Differential gene expression analysis was performed using the limma package (v3.56.2) in R (v4.3.1), employing empirical Bayes moderation to calculate log2 fold changes (log2FC) with corresponding adjusted p-values (FDR < 0.05). Genes were subsequently ranked by their log2FC values for downstream analyses.

Gene set enrichment analysis was conducted using clusterProfiler (v4.8.1) on both Hallmark gene sets (MSigDB v7.5.1) and KEGG metabolic pathways. The analysis generated normalized enrichment scores (NES) with statistical significance determined by Benjamini-Hochberg false discovery rate correction (FDR < 0.05). Metabolic pathway activity was further evaluated using the GSVA package with z-score transformation, and differential pathway activity between expression groups was assessed via limma.

To characterize the functional state of tumors, we analyzed 14 cancer-related functional signatures in CancerSEA using z-scores derived from GSVA and applied Lee et al.'s algorithm. The resulting scores were standardized (mean = 0, standard deviation = 1) to generate comparable functional state indicators. Finally, we analyzed the Pearson correlation between individual gene expression levels and functional state scores in the GSE112790 dataset.

Single-cell RNA-seq data processing

Through the Tumor Immune Single-cell Hub 2 (TISCH2), we accessed the GSE146115 hepatocellular carcinoma dataset and processed it with the MAESTRO pipeline to resolve RPL8 expression at single-cell resolution. After nonlinear dimensionality reduction via UMAP, cells were classified into malignant, stromal, and immune subsets, and RPL8 transcript levels were quantified within each compartment to delineate their cell-type-specific distribution.

Spatial transcriptomics analysis

We performed spatial transcriptomic profiling of liver cancer tissues using the Sparkle database (https://www.grswsci.top), a comprehensive pan-cancer spatial transcriptomics atlas integrating 10x Visium sequencing data [19,20]. Raw gene expression data were normalized using the NormalizeData function from the Seurat package. Spatial distribution patterns of gene expression and cell types were visualized through the SpatialFeaturePlot and SpatialPlot functions, respectively. To examine spatial relationships, we conducted Spearman correlation analysis between cellular composition and gene expression profiles, with results visualized using the linkET package. Tissue regions were classified based on malignant cell proportions: pure malignant (100 %), mixed (0–100 %), and normal (0 %) regions. For samples with limited spatial spots (< 30), we implemented a refined classification system (high-malignancy > 50 %, low-malignancy 0–50 %, normal 0 %) or a binary classification (malignant > 0 % vs non-malignant 0 %) when necessary. Differential gene expression analysis between regions was performed using Wilcoxon rank-sum tests, with results presented in bar plots to illustrate spatial expression characteristics.

Small molecule compound sensitivity analysis

To investigate potential therapeutic compounds targeting our gene of interest, we conducted comprehensive drug sensitivity analyses across multiple pharmacogenomic databases. Using Spearman correlation, we evaluated the association between gene expression levels and drug response metrics, including: 1) dose-response curve area under the curve (AUC) values from the CTRP and PRISM databases, and 2) half-maximal inhibitory concentration (IC_{50}) values from the GDSC1 and GDSC2 databases.

Generation of RPL8-knockdown stable cell lines

To establish stable RPL8-knockdown HUH7 hepatocellular carcinoma cell lines, we employed the Lipofectamine™ 3000 transfection system. Briefly, cells were plated in six-well plates and transfected with 5 μg of human shRPL8 plasmid using the manufacturer's recommended protocol. Following a 10–15 min incubation at room temperature to allow complex formation, the DNA-Lipofectamine mixture was added to cultured cells. After 48–96 h post-transfection, cells were subjected to selection with 2 μg/mL puromycin-containing complete medium for 3–5 days until complete death of non-transfected control cells was observed. The resulting puromycin-resistant polyclonal populations were expanded and cryopreserved for subsequent functional assays. Successful knockdown was verified by qPCR and western blot analysis prior to experimental use.

Cell culture and quantitative real-time PCR analysis

The human hepatocellular carcinoma cell line HUH7 (obtained from the Chinese Academy of Sciences Stem Cell Bank) was cultured in DMEM medium (Gibco, USA) supplemented with 10 % fetal bovine serum at 37 °C under 5 % CO_2. Total RNA was isolated using the HiPure Total RNA Mini Kit (Meiji Biotechnology, China) following the manufacturer's protocol, including cell lysis, ethanol precipitation, column purification, and elution. RNA quality and concentration were assessed using a Nanodrop 2000 spectrophotometer. Reverse transcription was performed with PrimeScript™ RT Premix (Takara, China), and RT-qPCR was carried out using TB Green® Premix Ex Taq™ II (Takara, China) on a LightCycler® 480 system (Roche, Switzerland). Gene-specific primers (ServiceBio) were used for amplification, and relative gene expression levels were calculated using the $2^{-\Delta\Delta CT}$ method. All experiments were performed in triplicate to ensure reproducibility.

Western blot analysis

Protein extraction was performed by lysing cells in RIPA buffer (Servicebio, China) containing protease inhibitor cocktail (Servicebio) on ice for 30 min. After centrifugation at 12,000 g for 15 min at 4 °C, protein concentrations were determined using a BCA protein assay kit (Servicebio). Equal amounts of protein were separated by 10 % SDS-PAGE and subsequently transferred to PVDF membranes (Millipore, USA). The membranes were blocked with 5 % non-fat milk (Servicebio) in TBST (Tris-buffered saline with 0.1 % Tween-20) for 1 h at room temperature, followed by overnight incubation at 4 °C with primary antibodies against RPL8 (1:10,000, Selleck, China) and HSP90 (1:10,000, Proteintech, China; loading control). After three washes with TBST, membranes were incubated with HRP-conjugated secondary antibodies (1:20,000, Zen-Bio, China) for 1 h at room temperature. Protein bands were visualized using enhanced chemiluminescence (ECL) substrate (Biosharp, China) and quantified using ImageJ software.

Cell proliferation and migration assay

Cell proliferation was detected using the CCK-8 method (UElandy, China): 5×10^3 cells were seeded into each well, and CCK-8 reagent was added at 0, 24, 48, and 72 h. After incubation for 2 h, the absorbance at 450 nm was measured. For the scratch assay, scratches were made using a 200 μL pipette tip, and cells were cultured in serum-free medium for 12–24 h. The migration width was analyzed using ImageJ.

Cell cycle analysis

Cells were harvested, washed once with ice-cold PBS, and resuspended in 1 mL DNA Staining Solution containing 10 μL Permeabilization Solution (Multi Sciences, China). After 30 min incubation at room temperature in the dark, samples were analysed by flow cytometry .

Cell-cycle distributions were modelled and quantified with ModFit LT v5.0.

Glutathione (GSH) measurement

Total intracellular glutathione levels were determined using a commercial GSH assay kit (Nanjing Jiancheng Bioengineering Institute, China) according to the manufacturer's protocol. Following cell lysis and protein precipitation, GSH concentration was measured spectrophotometrically and normalized to total protein content.

Statistical analysis

GraphPad Prism 10.0 software was used to perform one-way analysis of variance and *t*-tests. $p < 0.05$ indicated a statistically significant difference between the two groups.

Results

RPL8 is significantly overexpressed in hepatocellular carcinoma and demonstrates robust diagnostic potential

Integrated multi-omics analysis revealed that ribosomal protein RPL8 is markedly upregulated in HCC. TCGA transcriptomic data demonstrated that RPL8 mRNA levels were significantly elevated in HCC tissues compared to normal liver tissues ($p < 0.0001$; Fig. 2A). This finding was corroborated at the protein level by CPTAC pan-cancer analysis, which showed that RPL8 protein expression was consistently

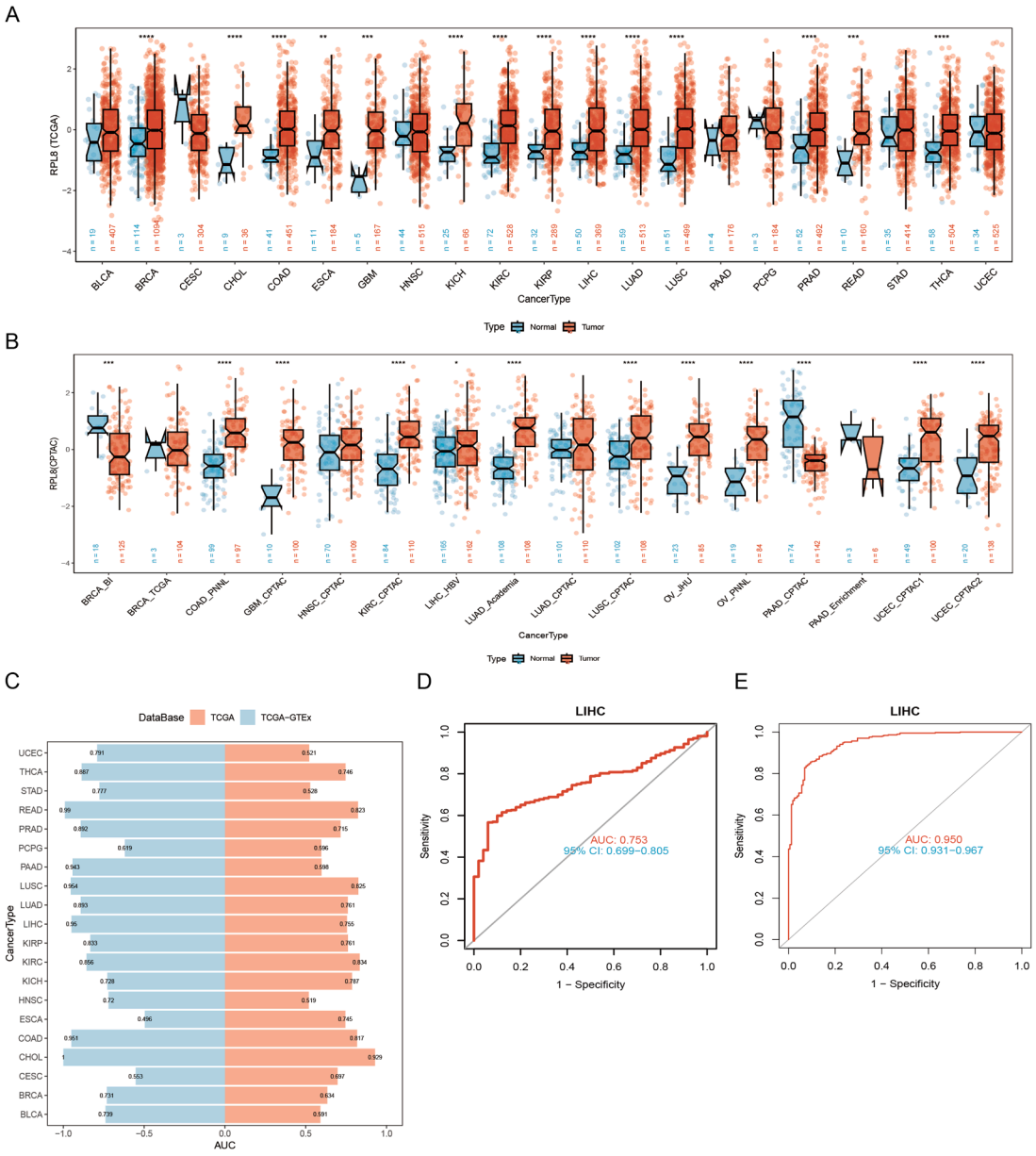

Fig. 2. Pan-cancer expression profile and diagnostic value of RPL8 in hepatocellular carcinoma.
(A) Comparative analysis of RPL8 mRNA expression levels across various cancer types and corresponding normal tissues from the TCGA database. (B) Protein expression patterns of RPL8 in pan-cancer analysis using CPTAC data. (C) Receiver operating characteristic (ROC) curves evaluating the diagnostic performance of RPL8 expression in discriminating tumor versus normal tissues (blue: TCGA-GTEx combined dataset; red: TCGA cohort). (D-E) ROC analysis demonstrating the diagnostic efficacy of RPL8 specifically for hepatocellular carcinoma in (D) TCGA-GTEx (AUC = 0.753, 95 % CI: [0.699 - 0.805]) and (E) TCGA datasets (AUC = 0.95, 95 % CI: [0.931 - 0.967]).(*$p < 0.05$, **$p < 0.01$, ***$p < 0.001$, ****$p < 0.0001$, ns: not significant).

higher in tumor tissues than in normal counterparts ($p < 0.05$; Fig. 2B).

To evaluate the diagnostic utility of RPL8, we performed receiver operating characteristic (ROC) curve analysis. Strikingly, RPL8 exhibited exceptional discriminatory power in distinguishing HCC from normal tissue, with an AUC of 0.95(95 % CI: 0.931 - 0.967) in the combined TCGA-GTEx dataset and 0.753(95 % CI: 0.699 - 0.805) in the independent TCGA cohort (Fig. 2C-E).

RPL8 expression correlates with adverse clinical outcomes in hepatocellular carcinoma

Our comprehensive analysis of TCGA clinical data revealed that elevated RPL8 expression significantly correlates with poor prognosis in HCC. Kaplan-Meier analysis demonstrated that high-RPL8-expression patients (red curves) exhibited worse overall survival (OS; $p < 0.021$; Fig. 3A), disease-specific survival (DSS; $p < 0.039$; Fig. 3B), progression-free interval (PFI; $p < 0.171$; Fig. 3C), and disease-free interval (DFI; $p < 0.075$; Fig. 3D) compared to low-expression counterparts (blue curves). Meta-analysis confirmed this association (pooled HR = 1.11,95 % CI: 1.02–1.21; $p < 0.05$;Fig. 3E) with moderate heterogeneity ($I^2 = 46$ %). Notably, multivariate Cox regression adjusting for age, gender, and TNM stage maintained RPL8 as an independent prognostic factor (HR > 1, $p < 0.05$; Fig. 3F), supporting its potential as a clinically valuable biomarker in HCC.

RPL8 promotes malignant phenotypes via cell cycle dysregulation and adaptive metabolism

Comprehensive pathway analysis demonstrated that RPL8 expression levels significantly influenced multiple oncogenic pathways in HCC (Fig. 4A). Notably, cell cycle-related pathways including MYC targets (NES > 1.7, FDR $q < 0.01$) and G2/M checkpoint regulation (NES > 1.7, FDR $q < 0.01$) were markedly enriched in RPL8-high tumors, as evidenced by bubble plot visualization where darker hues and larger diameters represented stronger enrichment. Metabolic profiling revealed RPL8-mediated reprogramming characterized by activation of glutathione metabolism ($p < 0.05$) and suppression of cytochrome P450-mediated drug metabolism ($p < 1e\text{-}05$; Fig. 4B). Further functional state correlation analysis showed (Fig. 4C) that RPL8 expression levels were significantly positively correlated with multiple malignant phenotypic characteristics, including cell cycle progression ($r = 0.45$, $p < 1.5e\text{-}10$), DNA damage response ($r = 0.48$, $p < 1.4e\text{-}11$), and DNA repair capacity ($r = 0.48$, $p < 1.1e\text{-}11$).

Single-cell RNA sequencing analysis revealed the expression and localization of RPL8 in HCC

Analysis of the GSE146115 single-cell RNA-seq dataset delineated the expression profile of RPL8 across the HCC tumor microenvironment. UMAP dimensionality reduction identified key cell populations, including malignant cells, monocytes/macrophages, and various immune cell subsets (Fig. 5A). Notably, RPL8 exhibited pronounced enrichment in malignant cells, with additional high expression observed in select immune populations, particularly $CD8^+$ *T* cells (Fig. 5B-D). Comparative analysis across three major cell subtypes confirmed significantly elevated RPL8 levels in malignant and immune cells relative to other cell types (Fig. 5E). Bar plot quantification further validated its preferential enrichment in malignant cells and $CD8^+$ *T* cells (Fig. 5F). Subpopulation analysis revealed a higher proportion of RPL8-positive cells within these populations (Fig. 5G), underscoring its cell type-specific expression pattern in HCC.

Spatial transcriptomic profiling reveals tumor-specific RPL8 expression patterns in hepatocellular carcinoma

Spatial transcriptomic profiling of HCC tissues revealed distinct

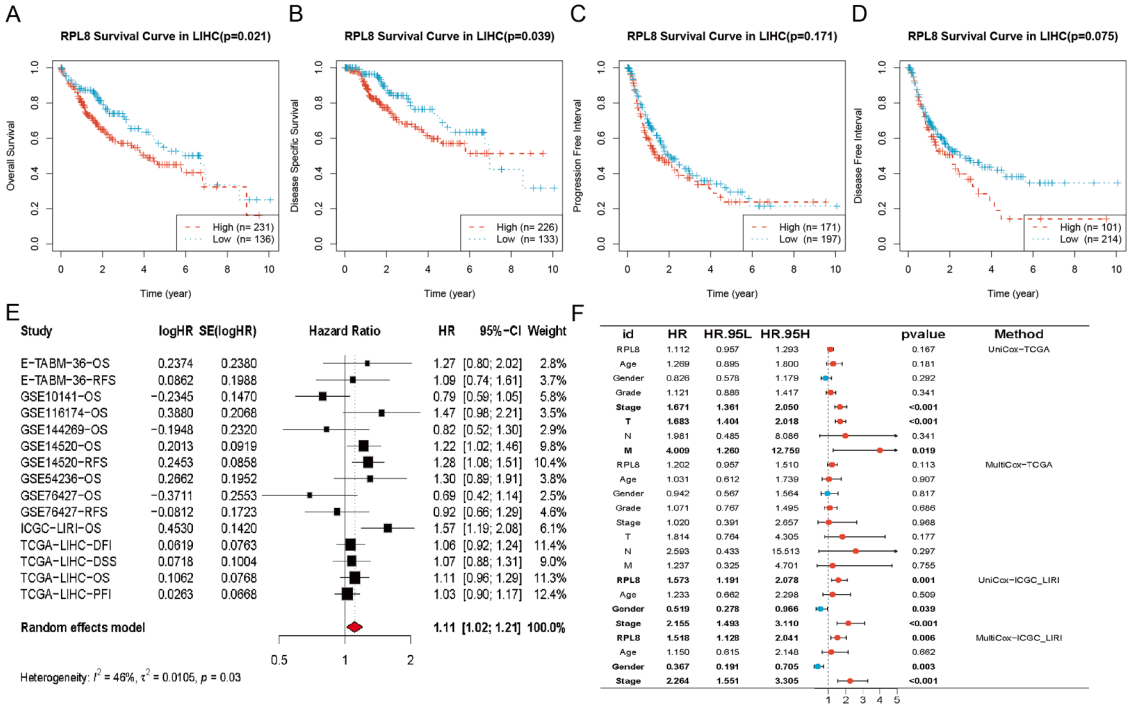

Fig. 3. Prognostic significance of RPL8 expression in hepatocellular carcinoma patients (Data from TCGA-LIHC).
(A) Kaplan-Meier analysis of overall survival (OS) stratified by RPL8 expression levels (high vs. low). (B) Disease-specific survival (DSS) curves comparing high and low RPL8 expression groups. (C) Progression-free interval (PFI) analysis based on RPL8 expression status. (D) Disease-free interval (DFI) outcomes according to RPL8 expression levels. (E) Forest plot of meta-analysis evaluating RPL8 expression and survival outcomes across multiple datasets. (F) Multivariate Cox proportional hazards model assessing independent prognostic factors, including RPL8 expression and clinical parameters.(*$p < 0.05$, **$p < 0.01$, ***$p < 0.001$, ****$p < 0.0001$, ns: not significant).

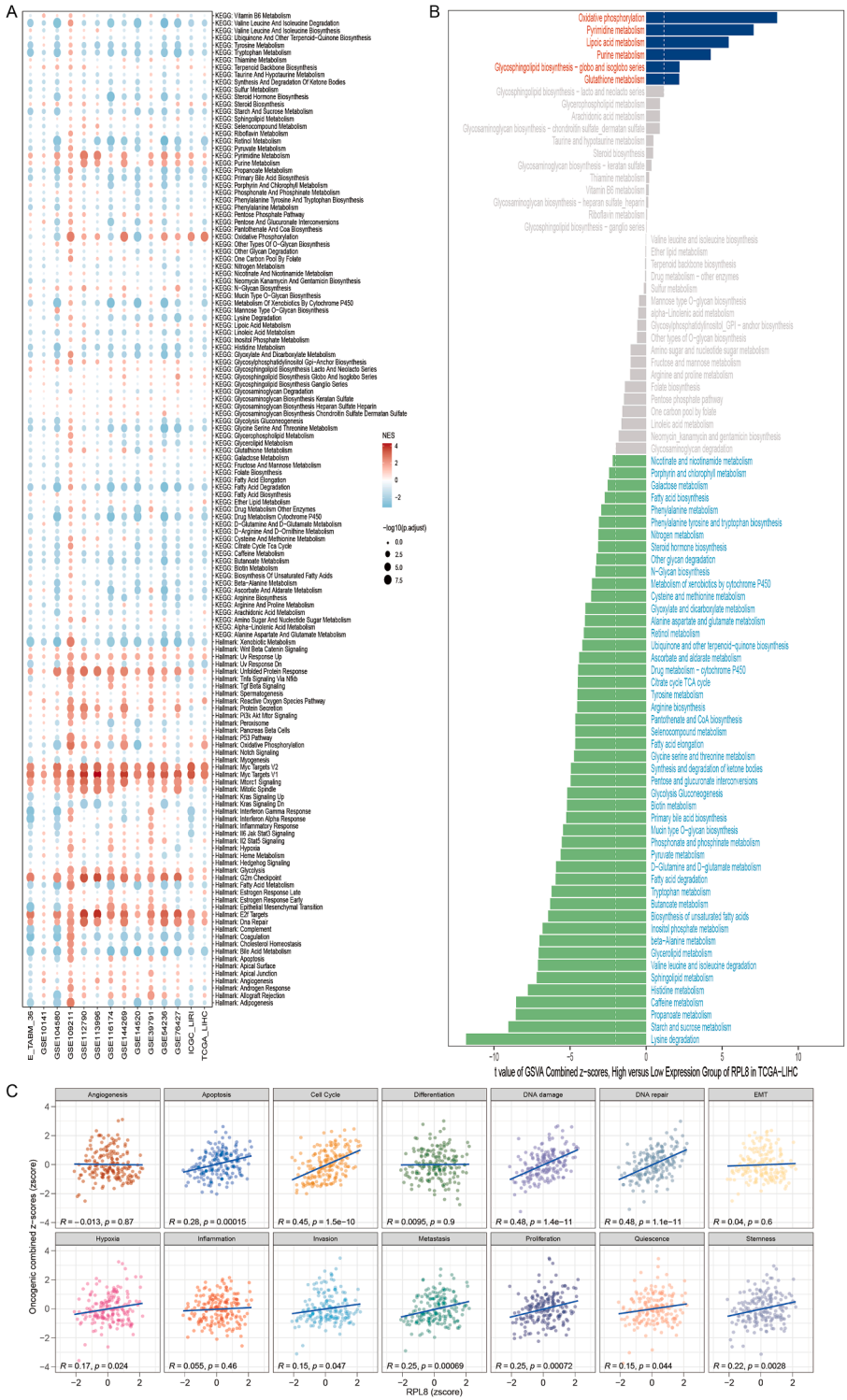

Fig. 4. Functional characterization of RPL8 in hepatocellular carcinoma progression (Data from TCGA-LIHC).
(A) Gene set enrichment analysis (GSEA) demonstrating differential pathway activation between RPL8-high and RPL8-low expression groups. (B) GSVA scores illustrating metabolic pathway alterations associated with RPL8 expression levels. (C) Correlation analysis between RPL8 expression and functional states in HCC.(*$p < 0.05$, **$p < 0.01$, ***$p < 0.001$, ****$p < 0.0001$, ns: not significant).

RPL8 expression patterns that closely mirrored tumor cell distribution (Fig. 6A and B). Quantitative analysis demonstrated significant enrichment of RPL8 expression in tumor regions compared to adjacent normal tissue ($p < 0.001$), with high-expression zones exhibiting precise colocalization with tumor cell clusters (Fig. 6C). Cellular deconvolution identified 12 distinct populations within the tumor microenvironment, including immune cell subsets ($CD4^+$ and $CD8^+$ *T* cells, NK cells, B cells, plasma cells, macrophages, and dendritic cells), stromal components (fibroblasts and endothelial cells), and parenchymal cells (hepatocytes and neutrophils).

Notably, spatial heterogeneity analysis revealed progressive RPL8 upregulation during tumor progression, with significantly higher

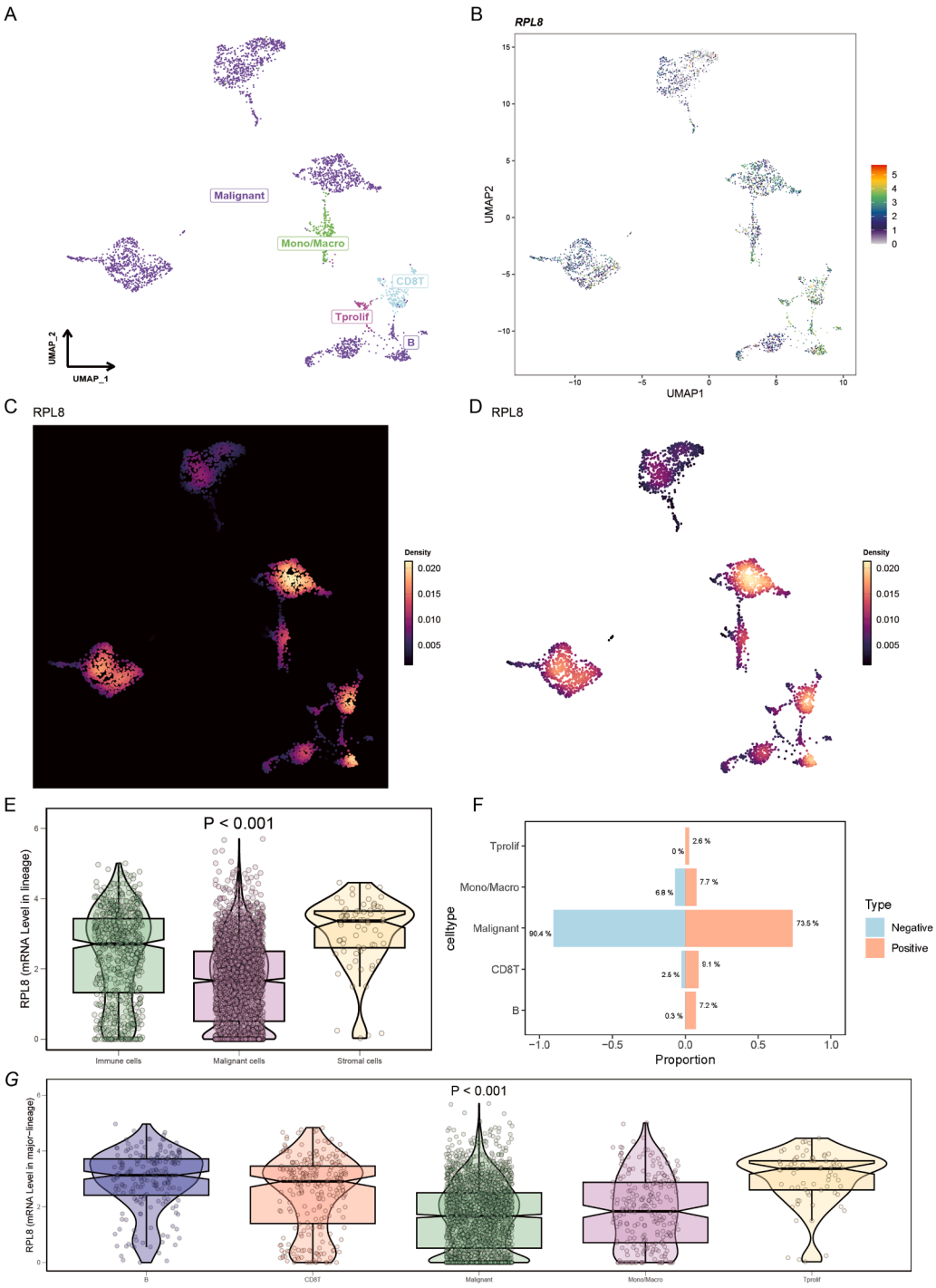

Fig. 5. Single-cell analysis of RPL8 expression in hepatocellular carcinoma (Data from GEO: GSE146115).
(A) UMAP visualization of major cell populations in HCC.(B-D) RPL8 expression patterns across cell clusters. (E) Violin plots showing elevated RPL8 expression in malignant and immune cells. (F) Proportion of RPL8-positive cells in different populations. (G) RPL8 expression comparison between immune and non-immune cells. (*$p < 0.05$, **$p < 0.01$, ***$p < 0.001$, ****$p < 0.0001$, ns: not significant).

expression in both malignant ($p < 0.001$) and transitional mixed regions ($p < 0.001$) compared to normal tissue (Fig. 6D). Correlation analysis demonstrated a strong positive association between RPL8 expression and tumor cells, while revealing significant negative correlations with multiple immune cell populations and stromal components (Fig. 6E).

RPL8 knockdown suppresses hepatocellular carcinoma cell proliferation and migration in vitro

To elucidate the functional role of RPL8 in HCC progression, we established stable RPL8-knockdown cell models. Successful RPL8 silencing was confirmed at both transcriptional and translational levels. Quantitative RT-PCR analysis revealed a significant reduction in RPL8 mRNA expression in shRPL8 cells compared to controls ($p < 0.001$; Fig. 7A). Consistent with this finding, Western blot analysis

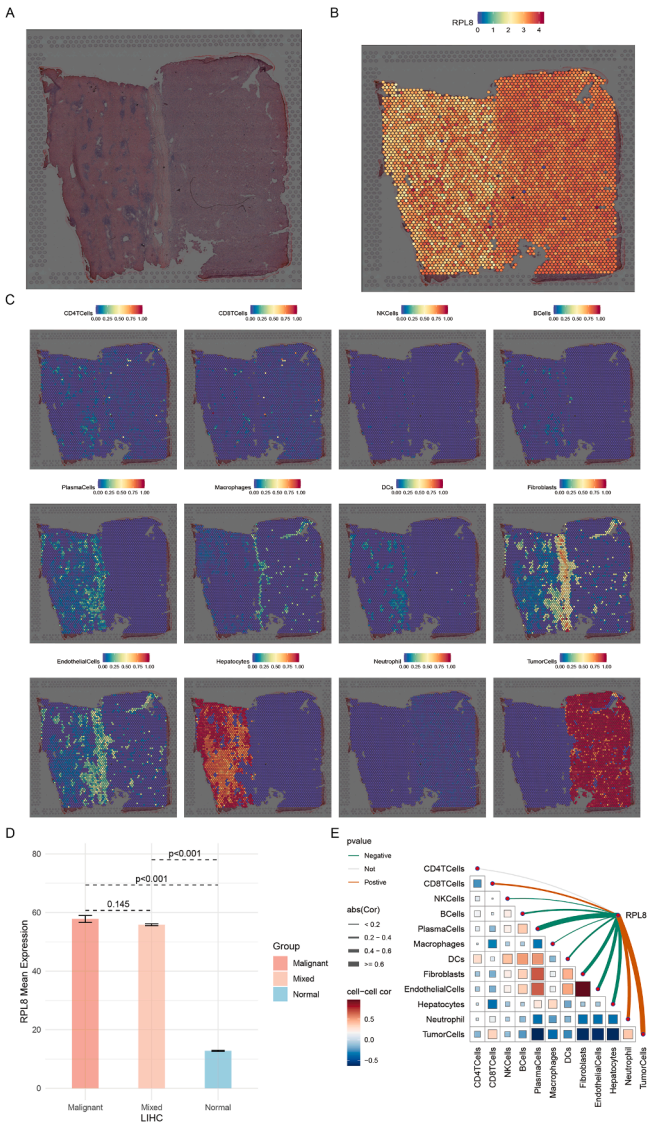

Fig. 6. Spatial transcriptomic profiling reveals RPL8 expression patterns in HCC. (A) Spatial transcriptomics of HCC tissue sections. (B) RPL8 expression mapping showing tumor-enriched distribution. (C) Cellular composition of HCC tumor microenvironment. (D) Differential RPL8 expression across malignant, mixed, and normal tissue regions. (E) Correlation heatmap of RPL8 expression with tumor microenvironment components.(*$p < 0.05$, **$p < 0.01$, ***$p < 0.001$, ****$p < 0.0001$, ns: not significant).

demonstrated markedly decreased RPL8 protein levels in knockdown cells ($p < 0.05$; Fig. 7B).

Functional characterization of RPL8-depleted cells revealed substantial impairment of malignant phenotypes. Wound healing assays showed significantly reduced migratory capacity in shRPL8 cells relative to controls ($p < 0.001$; Fig. 7C). Furthermore, CCK-8 proliferation assays indicated that RPL8 knockdown led to markedly decreased cell growth at both 48 h and 72 h time points ($p < 0.0001$; Fig. 7D). Metabolic analysis demonstrated that RPL8 silencing significantly suppressed glutathione production ($p < 0.05$; Fig. 7E), suggesting its involvement in redox regulation.

To investigate the underlying mechanism, we first performed cell cycle analysis by flow cytometry. RPL8 knockdown resulted in a significant accumulation of cells in the G2 phase (Fig. 7F), indicating that RPL8 is required for proper G2/M phase progression in HCC cells.

Consistent with the bioinformatics prediction linking RPL8 to MYC targets and G2/M checkpoint pathways (Fig. 4A), we examined the expression of key regulators by quantitative PCR. The mRNA levels of MYC, CDK1 (Cyclin-dependent kinase 1) , and CCNB1 (Cyclin B1) were all significantly downregulated in shRPL8 cells compared to controls (Fig. 7G).

Chemotherapeutic drug sensitivity analysis and small molecule compound prediction

Motivated by our finding that RPL8 activates the PI3K-AKT-mTOR and MYC signaling pathways (Fig. 4A), we hypothesized that RPL8 expression might dictate cellular sensitivity to pathway-targeted therapeutics. To test this, we performed a series of correlation analyses using the PRISM and CTRP drug sensitivity databases.

First, we conducted a Spearman correlation analysis between RPL8 expression and drug sensitivity (AUC) in the PRISM database. Our primary goal was to identify agents that aligned with our mechanistic hypothesis. This analysis revealed a significant positive correlation for sirolimus (an mTOR inhibitor) ($p < 0.01$), indicating that cells with high RPL8 expression are more resistant to sirolimus, and predicting that RPL8 knockdown would confer sensitivity (Fig. 8A). This finding provided a direct, hypothesis-driven candidate for functional validation.

In addition, the same unbiased screen identified other correlated compounds, including the natural product sclareol ($p < 0.01$). We noted sclareol as an exploratory candidate from a distinct therapeutic class, acknowledging that its mechanistic connection to the RPL8-associated pathways identified in this study is not predefined.

We further analyzed the correlation between RPL8 expression and drug AUC values in the CTRP database. Consistent with the PRISM results, this analysis showed that compounds including BRD-K24690302, lenvatinib (a multi-kinase inhibitor used in HCC), and CCT036477 were significantly and positively correlated with RPL8 expression ($p < 0.01$), again suggesting potential sensitization upon RPL8 depletion. In contrast, MK-1775, methotrexate, and BRD-K41597374 showed a significant negative correlation with RPL8 expression ($p < 0.01$;Fig. 8B).

To extend our analysis to conventional chemotherapeutic agents, we examined the GDSC1 and GDSC2 databases based on IC_{50} values. In the GDSC1 database, drugs such as RU-SKI, 43TAK-715, and 5-Fluorouracil showed a strong negative correlation with RPL8 expression ($p < 0.001$), suggesting that cells with RPL8 knockdown may be more resistant to these drugs (Fig. 8C). Similarly, in the GDSC2 database, compounds such as BMS-34,554, 1Wee1 inhibitor, and Linsitinib were significantly negatively correlated with RPL8 expression ($p < 0.001$) (Fig. 8D).

Based on the consistent computational prediction linking high RPL8 to mTOR pathway activity and sirolimus resistance, we sought to functionally validate this interaction. We performed dose-response assays using sirolimus on control and RPL8-knockdown (shRPL8) HUH7 cells. Strikingly, RPL8 knockdown profoundly sensitized HCC cells to sirolimus. The dose-response curve for shRPL8 cells exhibited a marked leftward shift compared to control cells (Fig. 8E). Quantitative analysis revealed that the half-maximal inhibitory concentration (IC_{50}) decreased from 75.1 μM in control cells to 52.16 μM in shRPL8 cells, confirming a significant increase in drug sensitivity upon RPL8 depletion.

Discussion

HCC remains a leading cause of cancer-related mortality worldwide. While the introduction of immune checkpoint inhibitor-based combinations has reshaped the first-line treatment landscape for advanced disease [16,17], a substantial proportion of patients derive limited or no benefit due to innate or adaptive resistance mechanisms [18]. This therapeutic challenge is compounded by persistent limitations in early diagnosis. The serum biomarker α-fetoprotein (AFP), despite being the clinical gold standard, has well-documented shortcomings including suboptimal sensitivity (30–40 % false-negative rate) and specificity (frequent elevation in benign liver conditions) [21]. Even when combined with des-γ-carboxy prothrombin (DCP) to improve accuracy, these

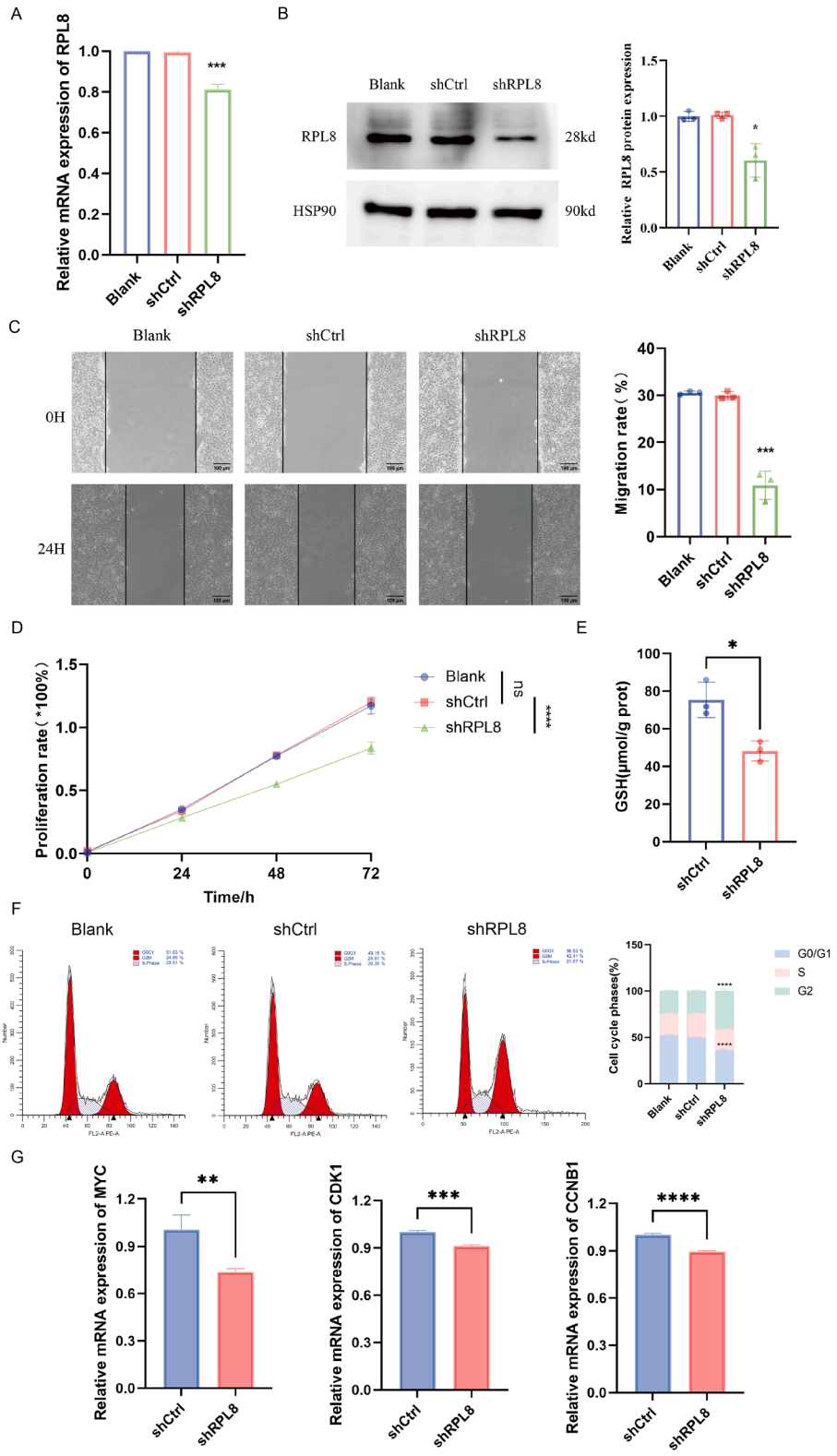

Fig. 7. Functional consequences of RPL8 knockdown in hepatocellular carcinoma cells.
(A) qRT-PCR analysis of RPL8 mRNA expression levels in control and shRPL8 cells. (B) Western blot analysis of RPL8 protein expression. (C) Wound healing assay demonstrating cell migration capacity. (D) CCK-8 assay assessing cell proliferation at 48 h and 72 h post-transfection. (E) Glutathione assay evaluating redox metabolism. (F) Flow cytometry analysis of cell cycle distribution in shCtrl and shRPL8 HUH7 cells. (G) qPCR analysis of MYC, CDK1, and CCNB1 mRNA levels in shCtrl and shRPL8 cells.(*$p < 0.05$, **$p < 0.01$, ***$p < 0.001$, ****$p < 0.0001$, ns: not significant).

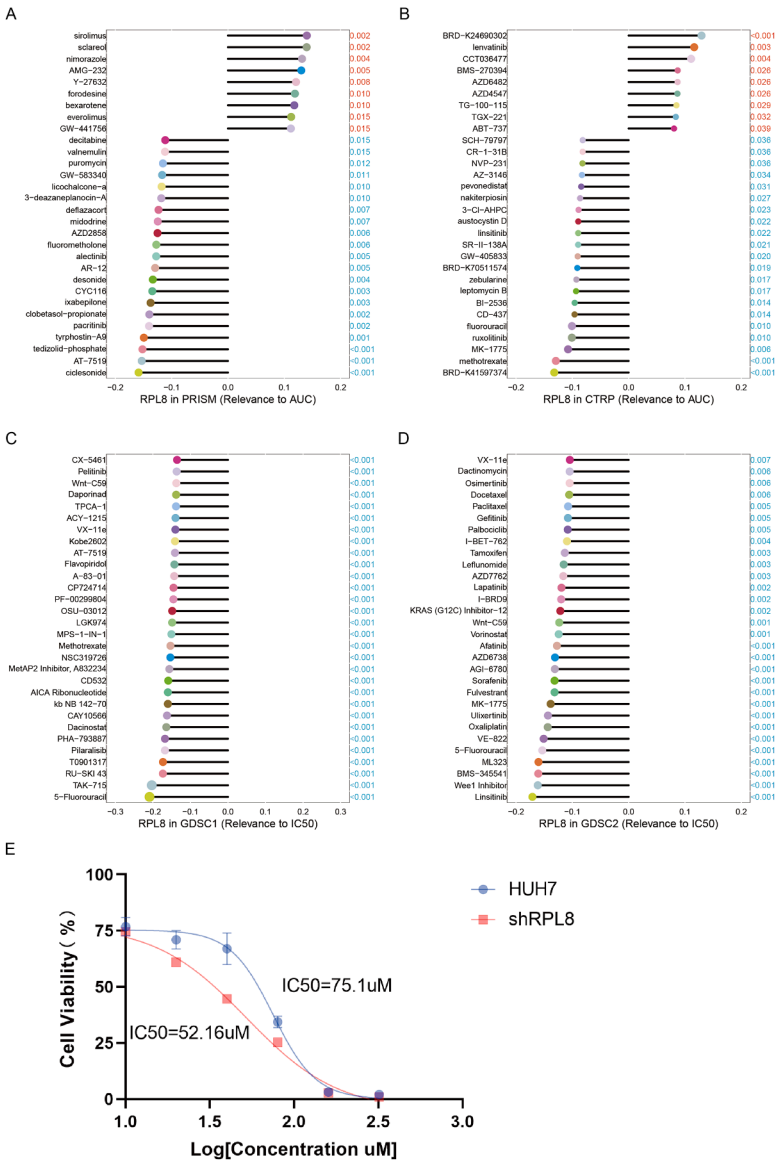

Fig. 8. Differential chemosensitivity analysis based on RPL8 expression levels. (A) Spearman correlation between RPL8 expression and drug AUC values in the PRISM database. (B) Spearman correlation between RPL8 expression and drug AUC values in the CTRP database. (C) Spearman correlation between RPL8 expression and drug IC_{50} values in the GDSC1 database. (D) Spearman correlation between RPL8 expression and drug IC_{50} values in the GDSC2 database. (E) Dose-response curves of shCtrl and shRPL8 HUH7 cells treated with sirolimus.(*$p < 0.05$, **$p < 0.01$, ***$p < 0.001$, ****$p < 0.0001$, ns: not significant).

markers largely reflect tumor burden rather than active disease biology [22,23]. In contrast, our study identifies ribosomal protein L8 (RPL8) as a multifunctional biomarker that addresses these dual gaps. It not only exhibits superior diagnostic performance (AUC = 0.95) but is also directly mechanistically involved in HCC pathogenesis. Unlike AFP, RPL8 actively regulates key oncogenic pathways—including mTOR signaling [12], metabolic reprogramming, and immune evasion—positioning it as a nexus connecting diagnosis with therapeutic targeting.

Recent advances in single-cell RNA sequencing (scRNA-seq) [23,24] and spatial transcriptomics [25,26] have revolutionized HCC research. These cutting-edge technologies have enabled us to precisely identify the distinct expression patterns of RPL8 in both malignant hepatocytes and $CD8^+$ *T* cells within the tumor microenvironment. This is further corroborated by spatial transcriptomic evidence demonstrating predominant KIAA1586 expression in malignant regions across multiple cancers, with single-cell analyses confirming its tumor-specific localization patterns [27]. Our spatial transcriptomic findings are further supported by recent studies identifying PRKDC as a dual-functional biomarker with both prognostic and therapeutic implications [28]. These collective findings underscore the transformative potential of multi-omics approaches in biomarker discovery. Moreover, they provide compelling evidence that ribosomal proteins, including RPL8, may play pleiotropic roles beyond canonical protein synthesis-modulating immune cell infiltration [29] and shaping cancer cell phenotypes through transcriptomic regulation [30].

Despite the comprehensive multi-omics integration and in vitro functional validation presented in this study, several limitations warrant consideration and indicate avenues for future investigation. First, the current findings largely rely on retrospective analysis of publicly available datasets and validation in a single hepatocellular carcinoma cell line. Consequently, prospective validation using independent, multicenter clinical cohorts is imperative to establish the translational relevance of RPL8 as a diagnostic and prognostic biomarker. Second, the absence of in vivo experimental models limits our ability to definitively ascertain the causal role of RPL8 in HCC tumorigenesis, metastatic

progression, and its modulation of the tumor immune microenvironment. Future studies employing patient-derived xenograft models or genetically engineered mouse models would provide critical insights into its functional impact in a physiologically relevant context. Third, although we have demonstrated that RPL8 knockdown enhances cellular sensitivity to mTOR inhibition and mechanistically linked this effect to the downregulation of MYC/G2M checkpoint signaling, the exact molecular interplay—particularly at the protein interaction or post-translational level—underlying this synergistic effect remains to be fully elucidated. Finally, methodological constraints inherent to spatial transcriptomics, such as tissue section depth and spatial resolution, may introduce variability into the interpretation of tumor–immune–stromal correlations. Furthermore, the correlative nature of these spatial data cannot distinguish whether RPL8 expression actively modulates the immune microenvironment or simply co-occurs with an immune-cold niche due to other underlying factors. Complementary approaches, including high-plex spatial proteomics or multiplex immunohistochemistry, could further refine our understanding of RPL8's spatial expression dynamics.

Additionally, while we have validated the single-agent sensitivity to sirolimus, the exploration of potential synergistic drug combinations involving RPL8 inhibition represents an important and distinct avenue for future therapeutic development.

In summary, addressing these limitations in subsequent research will substantially strengthen the translational foundation for evaluating RPL8 not only as a promising biomarker but also as a potential therapeutic target in hepatocellular carcinoma.

Stepping back from the individual datasets, a more integrative narrative around RPL8 begins to take shape. Our work positions it not simply as another upregulated gene in HCC, but as a multifunctional regulator operating at a critical juncture—where tumor cell-intrinsic signaling meets the immune microenvironment. Inside cancer cells, RPL8 sits at a fascinating crossroads, engaging both the proliferative drive (through MYC and G2/M checkpoint) and the adaptive metabolic network (via mTOR and glutathione pathways). This convergence suggests a vulnerability: targeting RPL8 might perturb this interconnected circuitry, offering a therapeutic advantage over single-pathway inhibition. Our functional data, showing synergism with mTOR blockade, provides a first glimpse into this potential.

Perhaps more intriguingly, our spatial and single-cell analyses hint at a role for RPL8 that extends beyond the cancer cell itself. Its specific enrichment in $CD8^+$ T cells and its spatial correlation with reduced immune infiltration led our team to consider a broader hypothesis: could RPL8 also be part of the machinery that helps tumors evade immune attack? This idea resonates with growing evidence that ribosomal proteins can moonlight in immune regulation [31]. While proving this causal link remains for future studies, this framework offers a parsimonious explanation for why high RPL8 marks both aggressive tumor biology and an immunologically suppressed niche. However, we must emphasize that this observed spatial correlation does not establish a direct causal mechanism. The association could be influenced by technical factors such as tissue section depth and immune infiltration gradients, or it may reflect a common association with a more aggressive tumor state. Our hypothesis that RPL8 might participate in immune evasion is thus presented as a plausible model consistent with the data, one that merits direct experimental validation in future studies.

From a translational standpoint, this dual perspective is particularly compelling. On one hand, RPL8 represents a therapeutic vulnerability within the tumor cell, and its expression could inform the use of mTOR pathway inhibitors. Our functional validation firmly establishes the mechanistic link between RPL8 and sensitivity to the mTOR inhibitor sirolimus. The observation with sclareol, while noted, remains preliminary and exploratory, requiring future work to elucidate any potential biological relationship with the RPL8-driven pathways we have characterized. This aligns with the ongoing search for predictive biomarkers to guide targeted therapy and overcome resistance [32]. On the other , its potential involvement in immune suppression raises the tantalizing prospect of a two-for-one therapeutic strategy—directly slowing tumor growth while potentially loosening the brakes on anti-tumor immunity. Such an approach is at the forefront of current efforts to modulate the tumor immune microenvironment for enhanced therapy efficacy [31]. Testing this will require moving into immunocompetent model systems.

We are, of course, mindful of the obvious challenge: targeting a ribosomal protein. The concern for on-target toxicity is real. However, the pronounced, tumor-specific overexpression we observe suggests a possible therapeutic window, consistent with the concept of "cancer-selective ribosomal addiction." Overcoming the delivery and specificity hurdles may require thinking beyond conventional inhibitors—towards strategies like targeted protein degradation (e.g., PROTACs) or context-dependent translation modulators.

In sum, our study reframes RPL8 from a passive biomarker to an active pleiotropic node in HCC pathogenesis. Its apparent involvement in both internal wiring and external communication of the tumor presents a complex but rich therapeutic target. We believe that pursuing this complexity—rather than avoiding it—could ultimately guide the development of more integrated treatment strategies for this challenging disease.

The clinical implications of our findings extend across the HCC care continuum. RPL8′s superior diagnostic performance could significantly improve early detection rates, particularly for AFP-negative cases that currently evade timely diagnosis. Its association with treatment response patterns suggests potential utility in guiding personalized therapy selection, while its involvement in immune modulation hints at possible applications in combination immunotherapy strategies. Most importantly, by elucidating RPL8′s multifaceted roles in HCC biology, our work provides not just another biomarker candidate, but a molecular nexus connecting several fundamental aspects of HCC pathogenesis - from ribosomal biogenesis to immune evasion - offering multiple avenues for therapeutic intervention that could ultimately improve outcomes for HCC patients worldwide.

Funding statement

This research was funded by the College Students' Innovation and Entrepreneurship Training Program of Guangxi University of Chinese Medicine, grant number 202410600024; the National Traditional Chinese Medicine Advantageous Specialty Construction Program, grant number GZYYYZH [2024]90; and the Guangxi Natural Science Foundation Project, grant numbers 2025GXNSFDA069035, 2025GXNSFAA069372.

Data availability

The raw RNA-seq (TPM) data for the TCGA-Liver Hepatocellular Carcinoma (TCGA-LIHC) cohort were generated by TCGA and downloaded from the NCI Genomic Data Commons portal (https://portal.gdc.cancer.gov, project ID TCGA-LIHC). Expression microarray or RNA-seq datasets under accession numbers GSE146115, GSE112790, GSE10141, GSE104580, GSE109211, GSE113996, GSE116174, GSE144269, GSE14520, GSE39791, GSE54236 and GSE76427 were obtained from the NCBI Gene Expression Omnibus (GEO, https://www.ncbi.nlm.nih.gov/geo). The E-TABM-36 series was retrieved from ArrayExpress (https://www.ebi.ac.uk/arrayexpress/experiments/E-TABM-36), and the ICGC-LIRI dataset from the International Cancer Genome Consortium (https://dcc.icgc.org/projects/LIRI-JP).

Ethics approval

Not applicable.

Clinical trial number

Not applicable.

Consent to publish declaration

Not applicable.

Consent to participate declaration

Not applicable.

CRediT authorship contribution statement

Jinna Tan: Writing – original draft, Visualization, Validation, Formal analysis, Data curation, Conceptualization. **Junzhu Liang:** Visualization, Investigation, Formal analysis, Data curation, Conceptualization. **Yaoyang Li:** Supervision, Software, Project administration, Investigation. **Jiaqian He:** Validation, Supervision, Software. **Hui Yin:** Supervision, Software, Investigation. **Hemeng Wu:** Supervision, Software, Project administration. **Yuzhen Luo:** Supervision, Software, Project administration. **Mingfen Li:** Writing – review & editing, Resources, Funding acquisition. **Fuli Long:** Resources, Funding acquisition. **Hongsheng Lin:** Writing – review & editing, Resources, Funding acquisition, Formal analysis.

Declaration of competing interest

(Article title: Integrated spatial and single-cell transcriptomics reveals RPL8 as a prognostic biomarker and therapeutic target in hepatocellular carcinoma)

All authors have completed the Elsevier declarations form.

The authors declare the following financial/personal relationships or interests that could be perceived as influencing the work:

Employment: None.

Consultancies: None.

Stock ownership: None.

Honoraria: None.

Paid expert testimony: None.

Patent applications/registrations: NoneGrants or other funding: This research was funded by the College Students' Innovation and Entrepreneurship Training Program of Guangxi University of Chinese Medicine, grant number 202,410,600,024; the National Traditional Chinese Medicine Advantageous Specialty Construction Program, grant number GZYYYZH [2024]90; and the Guangxi Natural Science Foundation Project, grant numbers 2025GXNSFDA069035, 2025GXNSFAA069372. The funders had no role in study design, data collection and analysis, decision to publish, or preparation of the manuscript.

Editorial role with the journal: None.

Acknowledgements

Not applicable.

Supplementary materials

Supplementary material associated with this article can be found, in the online version, at doi:10.1016/j.tranon.2025.102663.

References

[1] H. Sung, J. Ferlay, R.L. Siegel, M. Laversanne, I. Soerjomataram, A. Jemal, et al., Global Cancer statistics 2020: GLOBOCAN estimates of incidence and mortality worldwide for 36 cancers in 185 countries, CA Cancer J. Clin. 71 (2021) 209–249, https://doi.org/10.3322/caac.21660.

[2] K.O. Asafo-Agyei, H. Samant, Hepatocellular carcinoma. StatPearls, StatPearls Publishing, Treasure Island (FL), 2025.

[3] J.M. Llovet, R.K. Kelley, A. Villanueva, A.G. Singal, E. Pikarsky, S. Roayaie, et al., Hepatocellular carcinoma, Nat. Rev. Dis. Primer 7 (2021) 6, https://doi.org/10.1038/s41572-020-00240-3.

[4] S.A. Polyzos, L. Chrysavgis, I.D. Vachliotis, E. Chartampilas, E. Cholongitas, Nonalcoholic fatty liver disease and hepatocellular carcinoma:insights in epidemiology, pathogenesis, imaging, prevention and therapy, Semin. Cancer Biol. 93 (2023) 20–35, https://doi.org/10.1016/j.semcancer.2023.04.010.

[5] J. Wang, K. Qiu, S. Zhou, Y. Gan, K. Jiang, D. Wang, et al., Risk factors for hepatocellular carcinoma: an umbrella review of systematic review and meta-analysis, Ann. Med. 57 (2025) 2455539, https://doi.org/10.1080/07853890.2025.2455539.

[6] J.D. Yang, P. Hainaut, G.J. Gores, A. Amadou, A. Plymoth, L.R. Roberts, A global view of hepatocellular carcinoma: trends, risk, prevention and management, Nat. Rev. Gastroenterol. Hepatol. 16 (2019) 589–604, https://doi.org/10.1038/s41575-019-0186-y.

[7] M. Reig, A. Forner, J. Rimola, J. Ferrer-Fàbrega, M. Burrel, Á. Garcia-Criado, et al., BCLC strategy for prognosis prediction and treatment recommendation: the 2022 update, J. Hepatol. 76 (2022) 681–693, https://doi.org/10.1016/j.jhep.2021.11.018.

[8] J.A. Marrero, L.M. Kulik, C.B. Sirlin, A.X. Zhu, R.S. Finn, M.M. Abecassis, et al., Diagnosis, staging, and management of hepatocellular carcinoma: 2018 practice guidance by the American association for the study of liver diseases, Hepatol. Baltim. Md. 68 (2018) 723–750, https://doi.org/10.1002/hep.29913.

[9] K. Tzartzeva, J. Obi, N.E. Rich, N.D. Parikh, J.A. Marrero, A. Yopp, et al., Surveillance imaging and alpha fetoprotein for early detection of hepatocellular carcinoma in patients with cirrhosis: a meta-analysis, Gastroenterology 154 (2018) 1706–1718, https://doi.org/10.1053/j.gastro.2018.01.064, e1.

[10] J.R. Warner, K.B. McIntosh, How common are extraribosomal functions of ribosomal proteins? Mol. Cell 34 (2009) 3–11, https://doi.org/10.1016/j.molcel.2009.03.006.

[11] A. Ben-Shem, N. Garreau de Loubresse, S. Melnikov, L. Jenner, G. Yusupova, M. Yusupov, The structure of the eukaryotic ribosome at 3.0 Å resolution, Science 334 (2011) 1524–1529, https://doi.org/10.1126/science.1212642.

[12] T. Sun, W. Zhu, Q. Ru, Y. Zheng, Silencing RPL8 inhibits the progression of hepatocellular carcinoma by down-regulating the mTORC1 signalling pathway, Hum. Cell 36 (2023) 725–737, https://doi.org/10.1007/s13577-022-00852-9.

[13] M.L. Truitt, D. Ruggero, New frontiers in translational control of the cancer genome, Nat. Rev. Cancer 16 (2016) 288–304, https://doi.org/10.1038/nrc.2016.27.

[14] L. SUN, J. LI, B. YAN, Gene expression profiling analysis of osteosarcoma cell lines, Mol. Med. Rep. 12 (2015) 4266–4272, https://doi.org/10.3892/mmr.2015.3958.

[15] C. Zhou, W. Zhang, W. Chen, Y. Yin, M. Atyah, S. Liu, et al., Integrated analysis of copy number variations and gene expression profiling in hepatocellular carcinoma, Sci. Rep. 7 (2017) 10570, https://doi.org/10.1038/s41598-017-11029-y.

[16] A. Rizzo, A.D. Ricci, Challenges and future trends of Hepatocellular Carcinoma immunotherapy, Int. J. Mol. Sci. 23 (2022) 11363, https://doi.org/10.3390/ijms231911363.

[17] A. Rizzo, A.D. Ricci, G. Brandi, Trans-arterial chemoembolization plus systemic treatments for hepatocellular carcinoma: an update, J. Pers. Med. 12 (2022) 1788, https://doi.org/10.3390/jpm12111788.

[18] A. Rizzo, Locoregional treatments plus immunotherapy in hepatocellular carcinoma: where do we stand? Future Oncol. Lond Engl. 18 (2022) 1665–1668, https://doi.org/10.2217/fon-2021-1623.

[19] J. Shi, X. Wei, Z. Xun, X. Ding, Y. Liu, L. Liu, et al., The web-based portal SpatialTME integrates histological images with single-cell and spatial transcriptomics to explore the tumor microenvironment, Cancer Res. 84 (2024) 1210–1220, https://doi.org/10.1158/0008-5472.CAN-23-2650.

[20] Z. Xun, X. Ding, Y. Zhang, B. Zhang, S. Lai, D. Zou, et al., Reconstruction of the tumor spatial microenvironment along the malignant-boundary-nonmalignant axis, Nat. Commun. 14 (2023) 933, https://doi.org/10.1038/s41467-023-36560-7.

[21] C. Ayuso, J. Rimola, R. Vilana, M. Burrel, A. Darnell, Á. García-Criado, et al., Diagnosis and staging of hepatocellular carcinoma (HCC): current guidelines, Eur. J. Radiol. 101 (2018) 72–81, https://doi.org/10.1016/j.ejrad.2018.01.025.

[22] D.Y. Kim, B.N. Toan, C.-K. Tan, I. Hasan, L. Setiawan, M.-L. Yu, et al., Utility of combining PIVKA-II and AFP in the surveillance and monitoring of hepatocellular carcinoma in the Asia-Pacific region, Clin. Mol. Hepatol. 29 (2023) 277–292, https://doi.org/10.3350/cmh.2022.0212.

[23] D.W.-H. Ho, Y.-M. Tsui, L-K Chan, K.M.-F. Sze, X. Zhang, J.W.-S. Cheu, et al., Single-cell RNA sequencing shows the immunosuppressive landscape and tumor heterogeneity of HBV-associated hepatocellular carcinoma, Nat. Commun. 12 (2021) 3684, https://doi.org/10.1038/s41467-021-24010-1.

[24] S. Zhang, Z. Liu, D. Wu, L. Chen, L. Xie, Single-cell RNA-seq analysis reveals microenvironmental infiltration of plasma cells and hepatocytic prognostic markers in HCC with cirrhosis, Front. Oncol. 10 (2020) 596318, https://doi.org/10.3389/fonc.2020.596318.

[25] Y.-F. Wang, S.-X. Yuan, H. Jiang, Z.-X. Li, H.-Z. Yin, J. Tan, et al., Spatial maps of hepatocellular carcinoma transcriptomes reveal spatial expression patterns in tumor immune microenvironment, Theranostics. 12 (2022) 4163–4180, https://doi.org/10.7150/thno.71873.

[26] J. Ye, X. Gao, X. Huang, S. Huang, D. Zeng, W. Luo, et al., Integrating single-cell and spatial transcriptomics to uncover and elucidate GP73-mediated pro-angiogenic regulatory networks in hepatocellular carcinoma, Research 7 (2024) 0387, https://doi.org/10.34133/research.0387.

[27] J. Cheng, Z. He, Y. Liu, J. Jing, H. Zhang, Integrating machine learning and multi-omics to identify key SUMOylation molecular signature in sarcoma, Life Conflux 1 (2024), https://doi.org/10.71321/lcflx.00001 e88–e88.

[28] W. Pang, Y. Wang, X. Lu, M. Li, F. Long, S. Chen, et al., Integrated spatial and single cell transcriptomics identifies PRKDC as a dual prognostic biomarker and therapeutic target in hepatocellular carcinoma, Sci. Rep. 15 (2025) 14834, https://doi.org/10.1038/s41598-025-98866-4.

[29] R.K. Swoboda, R. Somasundaram, L. Caputo, E.M. Ochoa, P.A. Gimotty, F. M. Marincola, et al., Shared MHC class II-dependent melanoma ribosomal protein L8 identified by phage display, Cancer Res. 67 (2007) 3555–3559, https://doi.org/10.1158/0008-5472.CAN-06-2763.

[30] L. Xu, G. Yang, B. Song, D. Chen, A. Yunus, J. Chen, et al., Ribosomal protein L8 regulates the expression and splicing pattern of genes associated with cancer-related pathways, Turk J. Biol. Turk. Biyol. Derg. 47 (2023) 313–324, https://doi.org/10.55730/1300-0152.2666.

[31] E. Vitale, A. Rizzo, K. Santa, E. Jirillo, Associations between “cancer risk”, “inflammation” and “metabolic syndrome”: a scoping review, Biology. (Basel) 13 (2024) 352, https://doi.org/10.3390/biology13050352.

[32] O. Bas, T.K. Sahin, L. Karahan, A. Rizzo, D.C. Guven, Prognostic significance of the cachexia index (CXI) in patients with cancer: a systematic review and meta-analysis, Clin. Nutr. ESPEN. 68 (2025) 240–247, https://doi.org/10.1016/j.clnesp.2025.03.023.